Monthly Notices
of the
ROYAL ASTRONOMICAL SOCIETY

MNRAS **433,** 2054–2063 (2013)
Advance Access publication 2013 June 18

doi:10.1093/mnras/stt876

NPARSEC: NTT Parallaxes of Southern Extremely Cool objects. Goals, targets, procedures and first results

R. L. Smart,[1]⋆ C. G. Tinney,[2] B. Bucciarelli,[1] F. Marocco,[3] U. Abbas,[1] A. Andrei,[1,4] G. Bernardi,[1] B. Burningham,[3,4] C. Cardoso,[1] E. Costa,[5] M. T. Crosta,[1] M. Daprá,[1] A. Day-Jones,[1,5] B. Goldman,[6] H. R. A. Jones,[3] M. G. Lattanzi,[1] S. K. Leggett,[7] P. Lucas,[3] R. Mendez,[5] J. L. Penna,[4] D. Pinfield,[3] L. Smith,[3] A. Sozzetti[1] and A. Vecchiato[1]

[1]*Istituto Nazionale di Astrofisica, Osservatorio Astrofisico di Torino, Strada Osservatorio 20, 10025 Pino Torinese, Italy*
[2]*School of Physics, University of New South Wales, NSW 2052, Australia*
[3]*Centre for Astrophysics Research, University of Hertfordshire, Hatfield AL10 9AB, UK*
[4]*Observatório Nacional/MCT, R. Gal. José Cristino 77, CEP20921-400, RJ, Brazil*
[5]*Universidad de Chile, Camino el Observatorio 1515, Casilla 36-D, Santiago, Chile*
[6]*Max Planck Institute for Astronomy, Koenigstuhl 17, D-69117 Heidelberg, Germany*
[7]*Gemini Observatory, 670 N A'ohoku Place, Hilo, HI 96720, USA*

Accepted 2013 May 15. Received 2013 May 15; in original form 2013 February 14

ABSTRACT

The discovery and subsequent detailed study of T dwarfs have provided many surprises and pushed the physics and modelling of cool atmospheres in unpredicted directions. Distance is a critical parameter for studies of these objects to determine intrinsic luminosities, test binarity and measure their motion in the Galaxy. We describe a new observational programme to determine distances across the full range of T-dwarf subtypes using the New Technology Telescope (NTT)/SOFI telescope/instrument combination. We present preliminary results for ten objects, five of which represent new distances.

Key words: methods: data analysis – astrometry – parallaxes – proper motions – brown dwarfs.

1 INTRODUCTION

The prototype T dwarf was discovered in 1995 as a companion to the nearby M-dwarf star Gl 229 (Nakajima et al. 1995). This was rapidly followed by many discoveries in the near-infrared Two Micron All Sky Survey (hereafter 2MASS; Skrutskie et al. 2006) and the optical Sloan Digital Sky Survey (SDSS; York et al. 2000). Once discovered, significant efforts were undertaken to determine their distances (Dahn et al. 2002; Tinney, Burgasser & Kirkpatrick 2003, hereafter TIN03; Vrba et al. 2004) to map out the lower end of the Hertzsprung–Russell diagram and to constrain models. These early T-dwarf parallax programmes were operating in 'discovery' mode prioritizing new and exciting discoveries at cooler and cooler temperatures. For this reason, in 2010, the number of faint cool T6–T8 dwarfs with measured parallaxes was more than double the number of brighter hotter T0–T5 objects per subclass (∼5 versus ∼2, see Fig. 2).

The deeper United Kingdom Infrared Deep Sky Survey (UKIDSS; Lawrence et al. 2007) and the Canada–France Brown Dwarf Survey (CFBDS; Delorme et al. 2008b) programmes increased the number of known T dwarfs and extended the spectral range to T9. Recently, the *Wide-field Infrared Survey Explorer* (*WISE*; Wright et al. 2010) has extended the range into Y dwarfs and found a significant number of new T dwarfs. In 2010, this larger number of confirmed T dwarfs motivated us to commence an observational programme targeting parallax measurements spanning the full T-dwarf range: the NTT Parallaxes of Southern Extremely Cool objects (hereafter NPARSEC) survey.

NPARSEC's original goal was to obtain parallaxes for 65 new brown dwarfs to ultimately increase the number of objects with precisely measured parallaxes to 10 per T-dwarf subclass. This would allow us to reduce the uncertainty in spectroscopic parallaxes from the current level of 0.4 mag per subclass (Marocco et al. 2010) down to the level of the estimated cosmic scatter of 0.2 mag per subclass (Smart 2009). In practice, a higher-than-expected observing efficiency, combined with a significantly larger pool of bright T dwarfs discovered in the *WISE* survey, has enabled us to increase our NPARSEC survey sample to 85 targets.

This sample will be used to calibrate the absolute magnitude–spectral type relation that is critical for determining distances of larger samples used in the determination of the initial mass function and other statistical properties of the brown dwarf population. The distances will be used to discover and characterize peculiar

⋆E-mail: smart@oato.inaf.it

objects and unresolved binaries where the spectroscopic parallax relations for normal disc brown dwarfs are not reliable. Distances are also needed to characterize benchmark systems – e.g. systems that provide constraints on physical characteristics such as mass, age or metallicity – which, given the degeneracy between age and spectral type for brown dwarfs, are crucial to understand the various stages of T-dwarf evolution. The PARSEC programme (Andrei et al. 2011), being conducted by the same team, is a complementary programme for the hotter L brown dwarfs required to attain a complete picture of substellar objects.

In Section 2 we describe the observational programme, in Section 3 we present the target list, in Section 4 we present the reduction procedures used and a discussion of the precision attained, and in Section 5 we publish results from the first two years of observations and discuss individual objects. Finally in Section 6, we discuss the future of the programme and the relative merits of visitor and service mode observing for ground-based astrometry, with a view to the impact of *Gaia* (Perryman et al. 2001) and other large sky surveys currently underway.

2 OBSERVATIONAL PROGRAMME

2.1 Telescope and detector

Observations were carried out using the European Southern Observatory (ESO) 3.5 m New Technology Telescope (NTT) and its infrared spectrograph and imaging camera SOFI (Moorwood, Cuby & Lidman 1998). All observations were carried out in 'large field' mode, with a pixel scale of 0.288 arcsec pixel^{-1} and a field of view of 4.9 arcmin × 4.9 arcmin. Seeing is rarely better than 0.8, so the vast majority of images are well sampled with more than 3 pixels per full width at half-maximum. All observations were made in the *J* band which provides the best compromise between signal-to-noise and exposure time for these objects. As can be seen from Fig. 1, the SOFI *J* band is very similar to the 2MASS *J* band. This telescope and instrument combination has a proven track record for parallax determination (Neuhäuser et al. 2002; TIN03).

Our goal is to obtain at least 10 per cent distance precision on all targets. The largest distance expected for our targets is ≈50 pc,

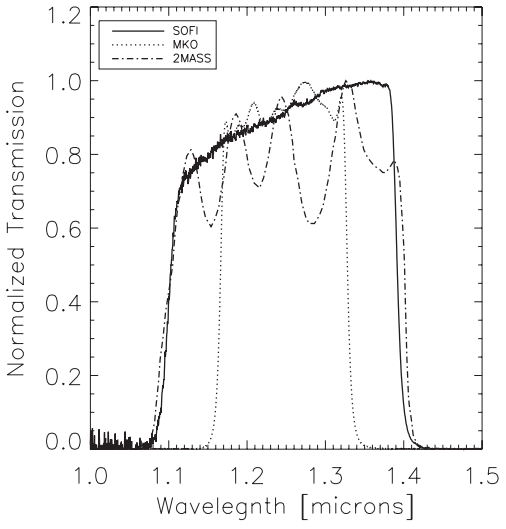

Figure 1. The SOFI *J* passband compared to the MKO and 2MASS bands all normalized to the maximum transmission and with no atmospheric absorption.

corresponding to a parallax of 20 mas and resulting in a net parallax precision requirement of 2.0 mas. Many targets – especially the latest ones – are much closer with an average distance of 20 pc where we will attain a relative precision of 4 per cent.

The parallaxes and proper motions are determined from the measured coordinates using the procedures in the Torino Observatory Parallax Program (hereafter TOPP; Smart et al. 2003). The parallax is determined from the equation

$$\xi_{n,m} = \xi_{n,m_o} + (t_m - t_{m_o})\mu_n + P_{\xi_m}\pi_n, \quad (1)$$

where $\xi_{n,m}$ is the position on frame m of star n in gnomic projection standard coordinates, $(t_m - t_{m_o})$ is the time difference with respect to the base frame, P_{ξ_m} is the parallax factor of observation m, and ξ_{n,m_o}, μ_n and π_n are the base frame position, proper motion and parallax of the star n. If we assume that the observations have a symmetric distribution of parallax factors, we find that the formal error in the ξ coordinate parallax from the covariance matrix of our observation equations is given by $\sqrt{\sigma_o^2/(N\langle P_{\xi_m}^2\rangle)}$, where N is the number of observations and σ_o is the sigma of unit weight of the least-squares adjustment. The parallax factor in ξ varies from -1 to 1; hence, with evenly distributed observations the mean $\langle P_\xi^2\rangle$ converges to 1/3, while for the coordinate parallel to declination on average it converges to 1/5. As the parallax can be found from both coordinates, the formal error simplifies to $\sigma_\pi \approx 1.5\sigma_o/\sqrt{N}$ or by rearranging $N \approx 2\sigma_o^2/\sigma_\pi^2$. To obtain a parallax error of 2 mas with a per epoch precision floor of 6–7 mas (see Section 4), we require 18–24 distinct epochs per target. We have therefore chosen as a mean goal obtaining 21 epochs per target.

Since the NTT is only operated in visitor mode, we optimized our target list to be as efficient as possible for full nights. Observations are scheduled on four nights spread over a seven-night period, i.e. one 2-night observing block, three nights with no observations, and then another 2-night observing block. On each 2-night observing block, we attempt to observe all objects on our target list near the meridian at least once, and then on the following 2-night block we repeat this sequence. The ability to split the observations over two nights allows a larger target list, improves the chances of getting at least one night without weather problems and permits us to tailor the target selection to observing conditions. For example, when seeing is poor, we concentrate on bright targets, or if the wind blows strongly from the north we concentrate on southern targets. In addition, observations on consecutive nights are of limited use, as the targets will not have moved significantly, and the general sky conditions and the instrumental setup will probably not have changed appreciably. However, between the two 2-night blocks our targets will have significantly moved: assuming an average target with a parallax of 50 mas and a proper motion of 500 mas yr^{-1}, the apparent motion will be 13 mas, i.e. more than twice our nominal precision.

The average night length in La Silla is 10.5 h so selecting targets evenly spaced in right ascension we observe on average 10.5/24, or 44 per cent, of our targets on each 2-night block. As we require 21 distinct epochs per target, we budget 21/2 runs per target, hence a total of 21/2 × 24/10.5 = 24 runs. We requested one observing run every 6–8 weeks for three years for a total of 96 nights which was granted by ESO starting 2010-10-01. This 'first-order' calculation does not take into account the differing night lengths, or seasonal weather differences. We have followed this plan over the first two years, and the number of observations to date (column N_E in Table 2) shows that the summer targets tend to have (on average) less epochs than the winter targets. In our current (and last) year of operation,

Table 1. Exposure times as a function of magnitude.

Magnitude J	DIT (s)	NDIT	N	Total time (min)
<14.0	3	20	9	9
14.0–15.0	10	6	9	9
15.0–16.0	20	6	9	18
16.0–17.0	30	4	9	18
17.0–18.0	30	4	18	36
>18.0	30	4	27	54

we will tailor time requests to 'round out' those objects requiring remedial treatment.

2.2 Observation procedures

During the day we collect darks to cover all possible exposure times. We obtain dome flats using the SOFI team *specialdomeflat* observing block, and each night we take sky flats. After sky flats are completed, we carry out an image analysis in the area of the first target to configure the NTT's meniscus mirrors. If the seeing is particularly good, or the images later in the night particularly elliptical, we redo this image analysis. It is usually possible to begin target observations after the first image analysis has been completed even though this is often before nautical twilight. During the twilight time we concentrate on brighter targets with shorter exposure times to minimize the effect of the brighter background sky.

The observation procedure starts with a short acquisition exposure and a move-target-to-pixel shift to (420, 420) – a point slightly off-centre in the SOFI focal plane which avoids trying to do astrometry at the boundaries between SOFI's four quadrant read-outs. We then begin a nine-point dither pattern similar to that adopted in TIN03. At each dither point, we take an exposure with detector integration time, DIT, repeated NDIT times and saved as a single co-added file. The telescope is then dithered and a new observation begun. This pattern is repeated N times (for $N = 9$, 18 or 27) to obtain a total integration (based on the target's published J magnitude) of DIT $\times$ NDIT $\times$ N, as shown in Table 1. This set of discrete exposure time combinations allows us to readily obtain the required dark frames in advance of each night. The total exposure times are conservative estimates to encompass a range of sky conditions and produce a signal-to-noise of at least 50 for the target in the final co-added image. Finding charts and observing block files were developed over the first few observing runs, and have remained substantially unaltered for the whole campaign.

2.3 Target scheduling

Splitting the target list over two nights allows us to tailor the observations to sky conditions. One driver for this split is the NTT active control of the primary and secondary mirrors. At the beginning of each night, we carry out an image analysis to attain the best mirror configuration for the current conditions. This is a costly process, taking 15–20 min, and the mirror shape remains partially a function of the altitude (elevation) of the telescope. We therefore split the targets into northern and southern groups and carry out the image analysis at the first target of the group for that night to obtain a configuration for the average elevation.

Nightly conditions often require us to override this grouping of targets, as when, for example, the NTT must observe downwind (when wind speeds lie between 12 and 15 m s^{-1}). Since the wind predominantly blows from the north, our split on north–south lines is systematically impacted by this restriction. Operationally, on the first night of a 2-night block, we attempt to observe the northern targets, wind permitting; if this is not possible, we concentrate on southern targets so that (wind permitting) we can observe the northern group on subsequent nights.

When seeing is particularly poor, the 'cost' of additional exposures to achieve a signal-to-noise of 50 for faint targets becomes prohibitive. In these conditions, we therefore concentrate on bright targets with short exposure times. This criterion dominates over other concerns, as the number of bright targets is such that we cannot pick and choose as we wish to obtain a north–south split.

3 TARGET LIST

The target list was chosen from all spectroscopically confirmed T dwarfs known in 2010 October (supplemented by a few additional late L dwarfs to fill gaps in the sky coverage). Fig. 2 shows the spectral type distribution of T dwarfs with published parallaxes with relative uncertainties of less than 10 per cent at three epochs: 2010, today and that expected at the conclusion of NPARSEC.

Our original goal was to deliver (in combination with extant published values) a total of at least 10 objects with measured parallaxes per spectral subclass. From Fig. 2 we can see that this will be possible for all but the first and last bins. The T0–T1 bins will have additional objects from the ESO 2.2 m PARSEC programme (Andrei et al. 2011), the Brown Dwarf Kinematics Project (hereafter BDKP; Faherty et al. 2012), the Hawaii Infrared Parallax Program (HIPP; Dupuy & Liu 2012) and the Carnegie Astrometric Planet Search (CAPS) programme (Shkolnik et al. 2012). The T9 and Y subtype bins will be filled by the UKIDSS follow-up parallax programme (UFPP; Smart et al. 2010) and the various *Spitzer* (Dupuy,

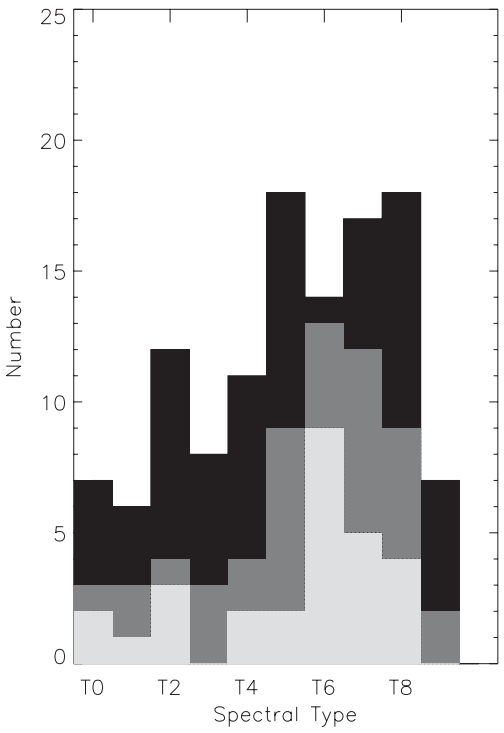

Figure 2. Number of T dwarfs with parallaxes published by 2010 in light grey, published today in dark grey and the expected NPARSEC contribution in black.

Kraus & Liu 2011; Kirkpatrick et al. 2012) and large telescope programmes (e.g. Tinney et al. 2012) currently underway.

In Table 2, we list our targets along with their published *J* magnitudes, infrared spectral types, estimated distances and discovery names from the original 2010 compilation. We used the published *J* magnitudes in the 2MASS system to derive exposure times. If the published *J* magnitude was in the MKO system, we use Stephens & Leggett (2004) to convert it to the 2MASS system. This magnitude and the spectral type–absolute magnitude relation of Marocco et al. (2010) is used estimate the photometric distances.

Table 2. NPARSEC targets. J is the published *J* magnitude available when the programme started in the 2MASS system unless indicated. The photometric distance, d_p, is calculated via the relation between absolute magnitude and spectral type provided in Marocco et al. (2010) and the *J* magnitude.

Short name	Discovery name	Ref dis.	Discovery α, δ h, deg (J2000)	J $\pm$ σ	Ref J	$d_p \pm \sigma$ (pc)	IR SpT	Ref SpT	N_E	ΔT (yr)
0024n00	ULAS J002422.94+002247.9	18	0.406 3721, 0.379 972 22	18.16 ± 0.07	30[a]	55 ± 8	T4.5	18	9	1.90
0034n05	2MASS J00345157+0523050	8	0.580 9916, 5.384 7222	15.53 ± 0.05	13	12 ± 2	T6.5	14	10	1.90
0050s33	2MASS J00501994−3322402	11	0.838 8722, −33.377 833	15.93 ± 0.07	13	12 ± 2	T7	14	11	1.90
0136n09	IPMS J013656.57+093347.3	15	1.615 7291, 9.563 1444	13.45 ± 0.03	13	6 ± 1	T2.5	15	9	1.90
0138s03	WISEP J013836.59−032221.28	28	1.643 4972, −3.372 5778	16.39 ± 0.10	13	25 ± 4	T3p	28	8	1.66
0148s72	WISEP J014807.25−720258.75	28	1.802 0139, −72.049 653	18.96 ± 0.07	28	9 ± 1	T9.5	28	9	1.68
0203s01	SDSS J020333.26−010812.5	9	2.059 2168, −1.136 6389	17.69 ± 0.04	30[a]	31 ± 4	L9.5	9	10	1.90
0223s29	WISEP J022322.34−293258.23	28	2.389 5388, −29.549 508	17.34 ± 0.15	28	14 ± 2	T8	28	7	1.66
0247s16	SDSS J024749.90−163112.6	13	2.797 1611, −16.520 333	17.19 ± 0.18	13	36 ± 6	T2 ± 1.5	13	10	1.90
0254n02	WISEP J025409.45+022359.1	27	2.902 6251, 2.399 7611	16.56 ± 0.16	27	10 ± 2	T8	28	6	0.81
0255s47	DENIS-P J0255−4700	1	2.917 6584, −47.014 136	13.25 ± 0.03	13	4 ± 1	L9	14	9	1.50
0310n16	2MASSW J0310599+164816	3	3.183 2943, 16.804 306	16.02 ± 0.08	13	16 ± 2	L9	14	12	1.89
0325n04	SDSS J032553.17+042540.1	13	3.431 4499, 4.427 9444	16.25 ± 0.14	13	20 ± 3	T5.5	13	10	1.90
0329n04	ULAS J0329+0430	29	3.488 9500, 4.506 8056	17.50 ± 0.03	30[a]	39 ± 6	T5	29	8	1.89
0348s60	2MASS J03480772−6022270	7	3.802 1443, −60.374 169	15.32 ± 0.05	13	9 ± 1	T7	14	9	1.17
0407n15	2MASS J04070885+1514565	8	4.119 1249, 15.249 028	16.06 ± 0.09	13	20 ± 3	T5	14	10	1.17
0415s09	2MASSI J0415195−093506	5	4.255 4278, −9.585 1667	15.69 ± 0.06	13	6 ± 1	T8	14	11	1.33
0423s04	SDSSp J042348.57−041403.5	6	4.396 8277, −4.234 3056	14.47 ± 0.03	13	9 ± 1	T0	14	9	1.58
0510s42	2MASS J05103520−4208140	17	5.176 4555, −42.137 406	16.22 ± 0.09	13	22 ± 3	T5	17	14	1.35
0516s04	2MASS J05160945−0445499	7	5.269 2919, −4.763 8611	15.98 ± 0.08	13	18 ± 3	T5.5	14	16	1.35
0518s28	2MASS J05185995−2828372	10	5.316 6528, −28.477 000	15.98 ± 0.10	13	19 ± 3	T1p	14	13	1.32
0528s33	WISEP J052844.51−330823.98	28	5.479 0306, −33.139 994	16.67 ± 0.09	28[a]	10 ± 1	T8:	28	12	1.12
0542s16	WISEP J054231.27−162829.16	28	5.708 6859, −16.474 767	16.58 ± 0.14	13	16 ± 2	T7-8:	28	14	1.12
0559s14	2MASS J05591914−1404488	2	5.988 6499, −14.080 222	13.80 ± 0.02	13	7 ± 1	T4.5	14	13	1.44
0611s04	WISEP J061135.13−041024.05	28	6.193 0919, −4.173 3472	15.49 ± 0.05	13	15 ± 2	T0	28	15	1.21
0612s30	WISEP J061213.89−303612.92	28	6.203 8584, −30.603 589	17.10 ± 0.19	28	12 ± 2	T8:	28	13	1.21
0623s04	WISEP J062309.93−045624.61	28	6.386 0917, −4.940 1694	17.51 ± 0.10	28	15 ± 2	T8	28	12	1.21
0627s11	WISEP J062720.07−111428.88	28	6.455 5750, −11.241 356	15.49 ± 0.05	13	10 ± 1	T7	28	13	1.19
0727n17	2MASSI J0727182+171001	5	7.455 0667, 17.167 000	15.60 ± 0.06	13	10 ± 1	T7	16	13	1.20
0729s39	2MASS J07290002−3954043	17	7.483 3388, −39.901 222	15.92 ± 0.08	13	7 ± 1	T8pec	17	15	1.21
0751s76	WISEP J075108.79−763449.6	28	7.852 4418, −76.580 444	19.34 ± 0.05	13	17 ± 2	T9	28	7	0.33
0817s61	DENIS J081730.0−615520	23	8.291 6698, −61.921 056	13.61 ± 0.02	13	5 ± 1	T6	23	9	1.13
0819s03	WISEP J081958.05−033529.01	28	8.332 7913, −3.591 3917	14.99 ± 0.04	13	13 ± 2	T4	28	17	1.32
0820n10	SDSS J082030.12+103737.0	13	8.341 7025, 10.627 000	16.98 ± 0.19	13	22 ± 4	L9.5 ± 2	13	14	1.32
0830n01	SDSS J083048.80+012831.1	9	8.513 5498, 1.475 3056	16.29 ± 0.11	13	23 ± 4	T4.5	14	13	1.32
0926n07	ULAS J092624.76+071140.7	25	9.440 2113, 7.194 6389	17.48 ± 0.02	30[a]	42 ± 6	T3.5	25	10	1.32
0939s24	2MASS J09393548−2448279	11	9.659 8558, −24.807 750	15.98 ± 0.11	13	7 ± 1	T8	14	14	1.44
0949s15	2MASS J09490860−1545485	11	9.819 0556, −15.763 472	16.15 ± 0.12	13	22 ± 3	T2	14	13	1.45
0950n01	ULAS J0950+0117	29	9.846 4670, 1.292 8611	18.05 ± 0.04	30[a]	19 ± 3	T8	29	15	1.46
1007s45	2MASS J10073369−4555147	17	10.126 025, −45.920 753	15.65 ± 0.07	13	17 ± 2	T5	17	12	1.44
1030n02	SDSS J103026.78+021306.4	9	10.507 439, 2.218 2500	17.14 ± 0.02	30[a]	24 ± 3	L9.5 ± 1	9	18	1.43
1048n09	SDSS J104829.21+091937.8	13	10.808 128, 9.327 0278	16.59 ± 0.15	13	27 ± 4	T2.5	13	14	1.36
1110n01	SDSSp J111010.01+011613.1	6	11.169 447, 1.270 2778	16.34 ± 0.12	13	21 ± 3	T5.5	16	13	1.36
1114s26	2MASS J11145133−2618235	11	11.247 592, −26.306 528	15.86 ± 0.08	13	9 ± 1	T7.5	14	12	1.38
1122s35	2MASS J11220826−3512363	11	11.368 961, −35.210 083	15.02 ± 0.04	13	13 ± 2	T2	14	13	1.37
1157n06	SDSS J115700.50+061105.2	9	11.950 136, 6.184 7778	17.08 ± 0.01	30[a]	33 ± 5	T1.5	14	13	1.24
1157n09	ULAS J115759.04+092200.7	22	11.966 400, 9.366 8611	16.84 ± 0.01	30[a]	31 ± 4	T2.5	22	12	1.36
1202n09	ULAS J120257.05+090158.8	25	12.049 181, 9.033 0000	16.80 ± 0.01	30[a]	28 ± 4	T5	25	10	1.37
1207n02	SDSS J120747.17+024424.8	4	12.129 769, 2.740 2500	15.58 ± 0.07	13	15 ± 2	T0	14	13	1.37
1209s10	2MASS J12095613−1004008	8	12.165 591, −10.066 889	15.91 ± 0.08	13	20 ± 3	T3	14	15	1.52
1215s34	2MASS J12154432−3420591	17	12.262 311, −34.349 850	16.24 ± 0.13	13	23 ± 4	T4.5	17	16	1.52
1300n12	ULAS J1300+1221	26	13.011 592, 12.354 083	16.69 ± 0.01	30[a]	7 ± 1	T8.5	25	12	1.31
1311n01	WISEP J131106.24+012252.4	28	13.185 066, 1.381 2222	19.16 ± 0.12	28	16 ± 2	T9:	28	10	0.47
1402n08	SDSS J140255.66+080055.2	13	14.048 789, 8.015 3611	16.84 ± 0.18	13	29 ± 5	T1.5	13	17	1.45

Table 2 – *continued*

Short name	Discovery name	Ref dis.	Discovery α, δ h, deg (J2000)	J $\pm \sigma$	Ref J	$d_p \pm \sigma$ (pc)	IR SpT	Ref SpT	N_E	ΔT (yr)
1404s31	2MASS J14044941−3159329	17	14.080 392, −31.992 517	15.58 ± 0.06	13	17 ± 2	T2.5	17	13	1.45
1459n08	ULAS J145935.25+085751.2	25	14.993 125, 8.964 2222	17.94 ± 0.03	30[a]	50 ± 7	T4.5	25	11	1.44
1504n10	SDSS J150411.63+102718.4	13	15.069 878, 10.455 422	16.50 ± 0.01	30[a]	15 ± 2	T7	13	11	1.31
1511n06	SDSS J151114.66+060742.9	13	15.187 406, 6.128 6389	16.02 ± 0.08	13	19 ± 3	T0 ± 2	13	10	1.44
1521n01	SDSS J152103.24+013142.7	9	15.350 908, 1.528 5000	16.40 ± 0.10	13	25 ± 4	T2:	14	10	1.14
1553n15	2MASSI J1553022+153236	5	15.883 966, 15.543 583	15.82 ± 0.07	13	11 ± 2	T7	14	11	1.29
1615n13	2MASS J16150413+1340079	17	16.251 146, 13.668 869	16.35 ± 0.09	13	19 ± 3	T6	17	11	1.38
1617n18	WISEP J161705.75+180714.0	28	16.284 929, 18.120 556	17.66 ± 0.08	28[a]	16 ± 2	T8	28	9	1.18
1630n08	SDSS J163022.92+081822.0	13	16.506 374, 8.306 1389	16.40 ± 0.11	13	22 ± 3	T5.5	13	11	1.38
1741n25	WISEP J1741+2553	28	17.690 071, 25.888 753	16.45 ± 0.10	28	4 ± 1	T9	28	10	1.20
1750n17	SDSSp J175032.96+175903.9	6	17.842 480, 17.984 500	16.34 ± 0.10	13	25 ± 4	T3.5	14	13	1.37
1812n27	WISEP J181210.85+272144.3	28	18.203 014, 27.362 306	18.19 ± 0.06	28[a]	15 ± 2	T8.5	28	7	1.18
1821n14	2MASS J18212815+1414010	24	18.357 819, 14.233 611	13.43 ± 0.02	24	10 ± 1	L4.5	24	7	1.20
1828s48	2MASS J18283572−4849046	8	18.476 589, −48.817 944	15.18 ± 0.06	13	12 ± 2	T5.5	14	14	1.90
1934s21	CFBDS J193430−214221	19	19.575 111, −21.705 833	16.77 ± 0.15	13	30 ± 5	T3.5	19	13	1.90
1936s55	2MASS J19360187−5502322	20	19.600 519, −55.042 278	14.49 ± 0.04	13	16 ± 2	L5	20	13	1.18
2018s74	WISEP J201824.98−742326.1	28	20.306 938, −74.390 581	17.10 ± 0.30	[b]	23 ± 5	T7	28	12	1.36
2043s15	SDSS J204317.69−155103.4	13	20.721 581, −15.850 861	16.62 ± 0.16	13	21 ± 3	L9	13	12	1.90
2047s07	SDSS J204749.61−071818.3	9	20.797 108, −7.304 8889	16.95 ± 0.20	13	29 ± 5	T0:	14	12	1.90
2052s16	SDSS J205235.31−160929.8	13	20.876 430, −16.158 556	16.33 ± 0.12	13	23 ± 3	T1 ± 1	13	12	1.90
2124n01	SDSS J212413.89+010000.3	9	21.403 852, 0.999 972 22	16.03 ± 0.07	13	20 ± 3	T5	14	13	1.90
2139n02	2MASS J21392676+0220226	20	21.657 436, 2.339 6389	15.26 ± 0.05	13	14 ± 2	T1.5	14	9	1.90
2151s48	2MASS J21513839−4853542	12	21.860 664, −48.898 389	15.73 ± 0.08	13	19 ± 3	T4	14	9	1.90
2154s10	2MASS J21542494−1023022	17	21.906 927, −10.383 950	16.42 ± 0.12	13	25 ± 4	T4.5	17	11	1.90
2228s43	2MASS J22282889−4310262	7	22.474 691, −43.173 942	15.66 ± 0.07	13	14 ± 2	T6	14	11	1.90
2229n01	ULAS J222958.30+010217.2	21	22.499 527, 1.038 1111	17.88 ± 0.04	30[a]	50 ± 7	T2.5	21	11	1.90
2239n16	WISEP J223937.55+161716.20	28	22.660 431, 16.287 833	16.08 ± 0.08	13	22 ± 3	T3	28	8	1.20
2325s41	WISEP J232519.54−410534.90	28	23.422 094, −41.093 028	19.75 ± 0.05	28[a]	20 ± 3	T9	28	7	1.18
2331s47	2MASS J23312378−4718274	8	23.523 272, −47.307 608	15.66 ± 0.07	13	17 ± 2	T5	14	9	1.90
2342n08	ULAS J2342+0856	29	23.708 048, 8.938 9167	16.37 ± 0.01	30[a]	17 ± 2	T6.5	29	13	1.90
2356s15	2MASSI J2356547−155310	5	23.948 547, −15.886 417	15.82 ± 0.06	13	17 ± 2	T5.5	14	8	1.67

J = *J*-band magnitude, ΔT = epoch range, d_p = photometric distance, N_E = number of epochs to date. Ref. – 1: Martin, Brandner & Basri (1999), 2: Burgasser et al. (2000), 3: Kirkpatrick et al. (2000), 4: Hawley et al. (2002), 5: Burgasser et al. (2002), 6: Geballe et al. (2002), 7: Burgasser, McElwain & Kirkpatrick (2003), 8: Burgasser et al. (2004), 9: Knapp et al. (2004), 10: Cruz et al. (2004), 11: Tinney et al. (2005), 12: Ellis et al. (2005), 13: Chiu et al. (2006), 14: Burgasser et al. (2006b), 15: Artigau et al. (2006), 16: Burgasser et al. (2006a), 17: Looper, Kirkpatrick & Burgasser (2007), 18: Lodieu et al. (2007), 19: Delorme et al. (2008a), 20: Reid et al. (2008), 21: Chiu et al. (2008), 22: Pinfield et al. (2008), 23: Artigau et al. (2010), 24: Kirkpatrick et al. (2010), 25: Burningham et al. (2010), 26: Goldman et al. (2010), 27: Scholz et al. (2011), 28: Kirkpatrick et al. (2011), 29: Burningham et al. (2013), 30: Skrutskie et al. (2006). Ref J notes: [a]magnitude on the MKO system; [b]estimated from the first NPARSEC observation.

4 REDUCTION PROCEDURES AND PRECISION

Flats, darks and biases are reduced using standard IRAF routines except for the dome flats where we use the SOFI team's IRAF script *special_flat.cl*. We co-add the separate dither images into one image per night using the *jitter* routine of the ECLIPSE (Devillard 1997) version 5.0 package. This routine corrects all frames using the flat-fields, darks and biases. For each object's dither sequence, it removes bright stars and makes the median of seven consecutive frames to use as a sky frame to clean each dither image separately. Finally it calculates pixel offsets between dithers and applies them to produce a re-sampled and co-added final image.

The determination of positions for inclusion in the parallax solution from this type of sequence can be done in multiple ways. The targets in the HIPP are sufficiently bright to enable generating one position estimate per dither. In the UFPP, the centroids are measured from the final combined image. Finally, the CAPS programme uses both approaches, with long integrations on the main field and a combination of short integrations on a window around the brighter targets to avoid saturation.

A naive consideration of the errors would suggest that the average of separate observations will be an improvement of $1/\sqrt{n}$ on the individual observations. However, this will only be true if each observation can be treated as an independent sample drawn from a random distribution. The processes that determine the astrometric precision of a given observation are complex and correlated within a single night. Therefore, there are good reasons not to expect precision to scale simply with $1/\sqrt{n}$ within a night, nor even potentially between nights.

When considered as an inter-night problem, the number of non-random factors is large: variable object fluxes, object distributions, atmospheric disturbances, optical distortions and the detector orientation/sensitivity will all contribute to correlate errors within a night. These aspects lead to a floor in the astrometric precision which multiple observations in the same night will not be able to reduce.

To test the precision of the different image treatment procedures, we examined the 27 dither observations of the two targets 0148s72 and 2325s41 on the three nights 2011-08-19, 2011-11-05 and 2011-11-10. We also evaluated four centroiding routines for these data: the two-dimensional Gaussian fitting procedure used in the TOPP,

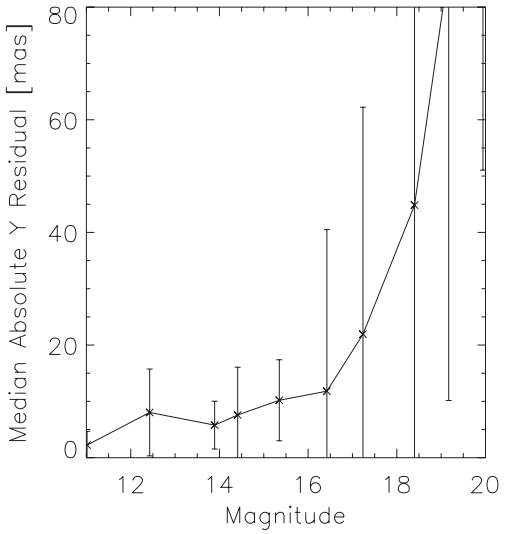

Figure 3. Absolute residuals of single dither observations for the field 0148s72 on the night of 2011-11-10 compared to the co-added image from the night of 2011-08-19. The solid line connects the median residuals in equal-magnitude bins.

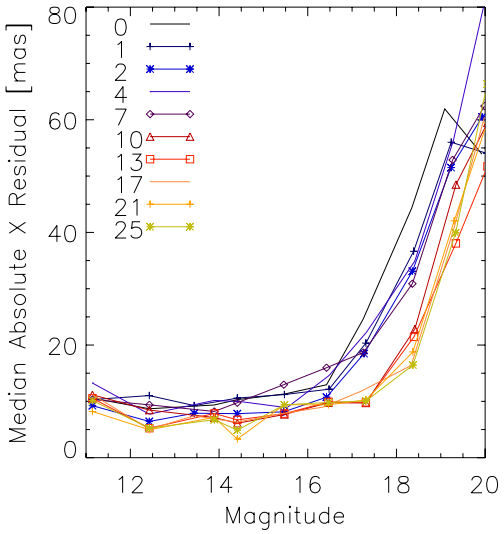

Figure 4. Absolute residuals of single dither observations (0 co-adds) and co-added combinations as shown in the legends of dithered observations for the field 0148s72 on the night of 2011-11-10 compared to the co-added image from the night of 2011-08-19.

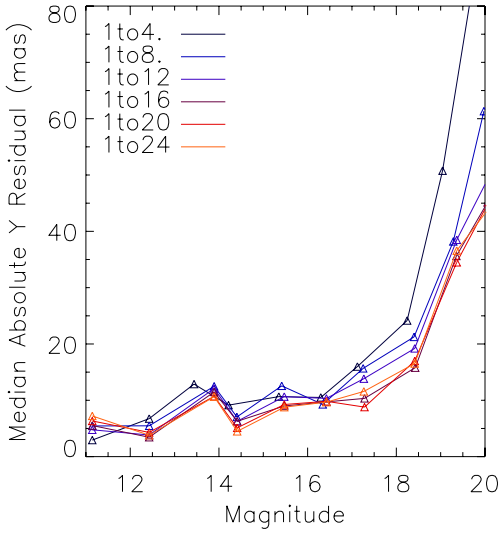

Figure 5. As Fig. 4 but with first co-added image always frame 1 and the number of co-added images shown in the legend.

the Cambridge Astrometry Survey Units *imcore* maximum likelihood barycentre (CASUTOOLS, v 1.0.21), the SExtractor's barycentre and the SExtractor's PSFEX point spread function fitting procedure (v. 2.8.6; Bertin & Arnouts 1996).

4.1 Precision: single dither observations

First we examine the centroiding precision for single dither images. We fit the positions from the 27 individual images for each night to the positions in the co-added image of the targets taken on 2011-08-19. In Fig. 3, we plot the median absolute residual in the Y coordinate for 27 frames reduced using the TOPP centroiding procedures for target 0148s72 on the night of 2011-11-10. The error bars represent the root mean square of the residuals about the median. At bright fluxes, there is a floor to the absolute residual of around 4–8 mas. At around $J = 14.5$, the residuals slowly rise up to 12 mas at $J = 16.5$, and thereafter deteriorate rapidly to 50 mas at $J = 18.5$. This deterioration is due to loss of signal-to-noise for the fainter objects. Similar results are seen on the other nights and for the other target (2325s41) – though the level of the precision floor at bright fluxes did vary significantly from 4 to 10 mas depending on the observing conditions. The precisions obtained in these comparisons were invariant to the centroiding routine used.

4.2 Precision: co-added observations

We now look at how the centroiding precision improves as a function of co-adding. In Fig. 4, we compare the single dither images and various co-added combinations for the 0148s72 2011-11-10 observations. The main improvement obtained is to push the deterioration in precision to fainter magnitudes, e.g. extending the precision floor from $J = 11$–15 (obtained with no co-adding) to $J = 11$–17 (with >10 co-added images). Considering only flux for 20 co-added images, we expect an increase of 3 mag; however, this procedure adds re-sampling noise so an increase of only 2 mag is reasonable.

Each co-added combination in Fig. 4 is made up of subsets where the first image varied and this may be a source of noise. We therefore also followed the change in precision when the first frame was kept constant. In Fig. 5, the first frame in the co-add is always frame 1 and the legend indicates the range of frames co-added. The sense of the results is similar to the previous test but it is cleaner because the first frame, and related systematic errors, is always in common. Note that we did not insist that the comparison objects are common to all tested sequences and this contributes to the noise seen.

4.3 Precision: co-added observations versus normal points

We now compare positions from co-added images to averages of the coordinates from single images. In this test we insist that the comparison objects are common to both comparisons, i.e. only the brighter objects detected in the single images. In Fig. 6, for the field 0148s72 on night 2011-11-05 we compare the positions from 27 co-added images, and the average of the 27 separate positions

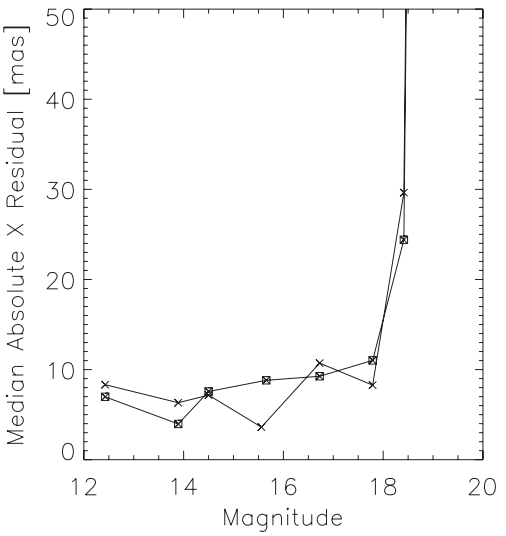

Figure 6. A comparison of 27 co-added images (squares) and the averages of the separate 27 images (crosses) for the field 0148s72 on the 2011-11-05 both compared to the co-added images of the same field on the night 2011-08-19.

to the observation of 2011-08-19. The two methods produce equal precision for the common objects and this indicates that the error floor is dominated by systematic, rather than random, errors.

4.4 Precision: conclusions

These tests are only valid for the NTT-SOFI system and reduction procedures employed here. In particular, we are still experimenting with drizzling and fractional pixel allocation co-adding procedures. We conclude that the improvement from multiple images in the precision floor is very modest, not $1/\sqrt{n}$, and the main improvement is to increase the magnitude range for that floor. This range does not increase in step with signal-to-noise probably because of noise introduced by the co-adding process. Finally, for the bright objects, the use of averaged separate observations is not better than using a co-added image of those separate observations.

In the results published here, we use the co-added images to maximize the magnitude range of the precision floor which we find to be around 6–7 mas. The exposures times are selected to ensure that all our targets achieve this precision.

5 PRELIMINARY RESULTS

In Table 3, we report preliminary results from the first two years of observations for 10 of our targets. The parallax determination procedures are substantially the same as those used in Smart et al. (2003). There are two differences in the application for this programme. (i) We do not correct for differential colour refraction as we are working in a wavelength region where this effect is negligible (Jao et al. 2011). (ii) The correction from relative to absolute parallax (COR in Table 3) is calculated using the model of Mendez & van Altena (1996) transformed into the *J* band which we conservatively estimate to have an error of 30 per cent (Smart, Lattanzi & Drimmel 1997). Five of the objects in Table 3 overlap with published targets (see Table 4). Our results are in reasonable agreement, with some exceptions which are discussed in the following subsections.

5.1 0310n16 (2MASSW J0310599+164816)

This object was seen as a binary in *Hubble Space Telescope* (*HST*) and VLT Nasmyth Adaptive Optics System Near-Infrared Imager and Spectrograph observations (Stumpf et al. 2010) with a separation of 200 mas. In Stumpf at al. they adopted a spectroscopic distance of 25 pc, and assuming a face-on circular orbit this would imply a 5.2 au separation. From the change in position angle of 15°.5, they found a period of 72 yr and hence a minimum system mass of 30 $M_{\rm Jup}$. This low mass would imply a very young system, as an older system would have to be more massive to be still close to the L/T boundary. However, the hypothesis of a young age is not supported by a comparison of the space velocities to the locus of known young objects as done in Marocco et al. (2010), and in an examination of the Burgasser (2007) spectrum we do not see the triangular *H* band, nor a significant *H*- and *K*-band flux enhancement, that we expect from young objects (e.g. Lucas et al. 2001). This low-mass, and hence young-age, constraint will be relaxed if the orbit is larger than estimated above, which will be the case if the system is inclined or if the distance is larger than assumed by Stumpf et al. Our trigonometric distance measurement is $27.1^{+3.7}_{-2.3}$ pc, larger than the adopted 25pc but not enough to change the overall conclusion.

5.2 1828s48 (2MASS J18283572−4849046)

This object is in the BDKP programme but observed over a period before NPARSEC began. We find that our parallax and proper motions (87.9 ± 2.0 mas, 234.6 ± 2.5 mas yr^{-1}, 88.3 ± 2.6 mas yr^{-1}) agree with those found in the BDKP (83.7 ± 7.7 mas, 231.4 ± 0.5 mas yr^{-1}, 52.4 ± 10.9 mas yr^{-1}) with the exception of the declination proper motion. This could be due to the short epoch coverage for both programmes (1.91 yr for NPARSEC and 1.88 yr for BDKP). The difference could also be due to orbital motion if the object turns out to be a binary. However, this is unlikely as the photometric distance is the same as the astrometric one so the object does not appear overluminous.

5.3 2047s07 (SDSS J204749.61−071818.3)

In the BDKP this object was observed on six nights over 1.34 yr and parallax and proper motions of 49.9 ± 7.9 mas, 48.7 ± 11.2 mas yr^{-1} and -193.8 ± 11.2 mas yr^{-1} were found, while in NPARSEC with 11 nights over 1.91 yr we find 33.2 ± 5.5 mas, 35.9 ± 5.2 mas yr^{-1} and -241.1 ± 5.0 mas yr^{-1}. This object has a 2MASS *J* magnitude of 16.95 so it is at the faint end of the exposure bin for $J = 16$–17 in Table 1; hence, the signal-to-noise was often close to the minimum acceptable. As shown in Fig. 7, the solution is (not unexpectedly) noisy. Notwithstanding this lower precision the fit appears well constrained and we note that the photometric distance is 29 ± 5 pc which supports the NPARSEC value.

5.4 2139n02 (2MASS J21392676+0220226)

Faherty et al. (2009) find proper motions of $+507 \pm 22$ and 123 ± 22 mas yr^{-1}, consistent with the values found in this programme. Radigan et al. (2012) and Khandrika et al. (2013) find evidence of a 7 h *J*-band variability that we will search for when we have a larger observational data set. Burgasser et al. (2010) indicate this object as a strong binary L/T candidate; however, based on our distance, it does not appear to be particularly bright and the residuals to the solution shown in Fig. 7 show no signatures of orbital motion. Hence, these observations do not support the binarity hypothesis. In

Table 3. Preliminary parallaxes and proper motions for NPARSEC targets.

NPARSEC name	RA (h:m:s)	Dec. (°:′:″)	Epoch (yr)	Absolute π (mas)	COR (mas)	μ_α (mas yr^{-1})	μ_δ (mas yr^{-1})	$N\star$, N_e	ΔT (yr)
0310n16	3:11:00.0	+16:48:15.3	2011.64	36.9 ± 3.4	1.58	245.9 ± 4.0	6.2 ± 3.3	78, 12	1.89
1828s48	18:28:36.0	−48:49:03.7	2012.58	87.9 ± 2.0	0.83	234.6 ± 2.5	88.3 ± 2.6	278, 13	1.91
2043s15	20:43:17.7	−15:51:04.3	2011.62	22.8 ± 4.7	1.32	43.7 ± 4.8	− 109.4 ± 3.1	173, 12	1.91
2047s07	20:47:49.5	−7:18:21.8	2012.58	33.2 ± 5.5	1.47	35.9 ± 5.2	− 241.1 ± 5.0	155, 11	1.91
2139n02	21:39:27.1	+2:20:23.9	2012.44	101.5 ± 2.0	1.36	485.9 ± 2.0	124.8 ± 2.7	86, 9	1.91
2151s48	21:51:38.8	−48:53:56.5	2010.76	60.0 ± 3.8	1.61	414.7 ± 3.5	− 201.7 ± 4.5	52, 9	1.90
2154s10	21:54:25.1	−10:23:01.6	2010.75	37.2 ± 3.5	1.62	258.0 ± 3.1	63.3 ± 5.3	54, 11	1.91
2228s43	22:28:29.0	−43:10:30.4	2011.85	92.1 ± 2.6	1.46	51.7 ± 3.2	− 301.3 ± 1.6	18, 11	1.91
2342n08	23:42:28.9	+8:56:20.0	2010.75	34.3 ± 5.1	1.59	264.1 ± 4.4	− 52.6 ± 3.0	56, 13	1.91
2356s15	23:56:54.3	−15:53:18.5	2010.75	57.9 ± 3.5	2.21	− 430.3 ± 5.8	− 607.9 ± 3.0	35, 8	1.67

COR = correction to absolute parallax, N_* = number of reference stars, N_e = number of epochs and ΔT = epoch range.

Table 4. Objects with previously published parallaxes.

NPARSEC name	NPARSEC parallax	Literature parallax	Reference
1828s48	87.9 ± 2.0	84.0 ± 8.0	BDKP
2047s07	33.2 ± 5.5	49.9 ± 7.9	BDKP
2151s48	60.0 ± 3.8	50.4 ± 6.7	BDKP
2228s43	92.1 ± 2.6	94.0 ± 7.0	BDKP
2356s15	57.9 ± 3.5	69.0 ± 3.0	BDKP
"	"	74.4 ± 5.8	Vrba et al. (2004)

addition, Radigan et al. (2012) ruled out binarity at distances beyond the 1.56 au level using *HST*/NICMOS imaging, and Khandrika et al. (2013) do not find any significant variations in radial velocities using Gemini/NIRSPEC observations.

5.5 2342n08 (ULAS J2342+0856)

This object was provided internally from the UKIDSS T-dwarf search and spectroscopically typed as a T6.5. In Scholz (2010), based on photometry, this target was indicated as a probable T7 with proper motions of +229 ± 55 and −9 ± 9 mas yr^{-1}. These proper motions are inconsistent with the NPARSEC values of 264.1 ± 4.4 and −52.6 ± 3.0 mas yr^{-1}, but in his discussion Scholz estimates the expected error of this object to be 48 mas yr^{-1} (see his table 5); using this value the two estimates become formally consistent.

5.6 2356s15 (2MASSI J2356547−155310)

The NPARSEC parallax (57.9 ± 3.5 mas) is significantly smaller than the published values (69.0 ± 3.0 and 74.4 ± 5.8 mas) while the NPARSEC proper motions (−430.3 ± 5.8 and −607.9 ± 3.0 mas yr^{-1}) are in the middle of inconsistent published values (−422.7 ± 4.0 and −615.9 ± 3.6 mas yr^{-1} in BDKP and −443 ± 2 and −600 ± 2 mas yr^{-1} in Vrba et al. 2004). This target has the shortest NPARSEC temporal coverage (1.61 yr) and the lowest number of observations (8) in this sample so we will wait for more observations before investigating further or drawing conclusions on the difference between the published and NPARSEC values.

6 GENERAL PROGRAMME CONSIDERATIONS

6.1 Visitor versus service programmes

It is useful to compare the NPARSEC visitor programme to a service programme such as the UFPP. Service programmes provide

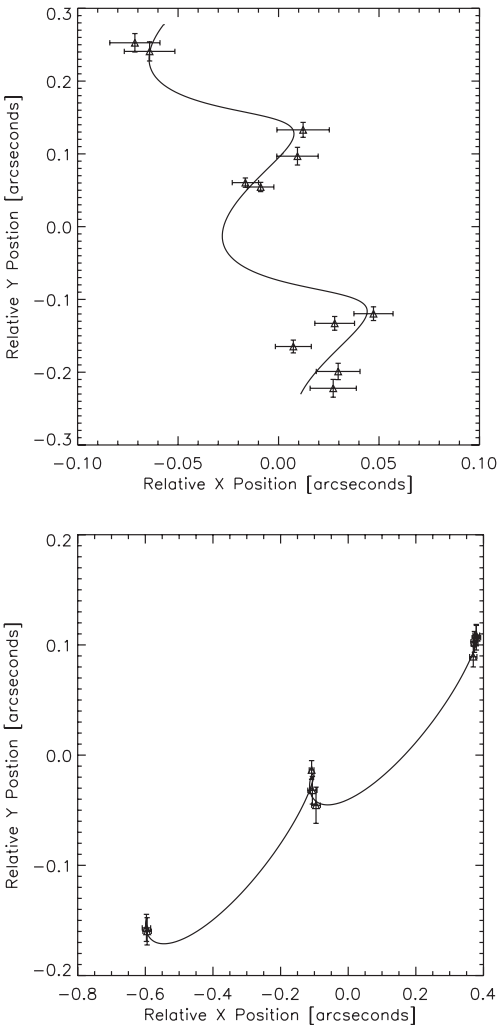

Figure 7. Example target solutions. Top panel: 2047s07 with the highest error; lower panel: 2139n02 lowest error.

two paths to increase the value of observations for a parallax determination: a flexibility to micro-manage scheduling and an ability to match observations to conditions.

Scheduling flexibility in parallax observations usually translates into a request for observations at twilights when the parallax factor is an absolute maximum in ecliptic longitude, but this is also the point where the parallax factor in the ecliptic latitude is a minimum.

This is justified because the parallax factor in longitude has a larger range, the factor in latitude being usually visible at only one extreme and modulated by the sine of the latitude. However, modern programmes use both coordinates to determine parallaxes so this is not a particularly strong benefit. Another plus from scheduling flexibility is, if the programme is ranked high enough, to obtain a more uniform observation distribution. In NPARSEC there are seasons when we only have two observations of a target; in the UFPP, where our programme has a high priority, we obtain over 90 per cent of the observations requested.

Having conditions that match our requirements is undeniably an advantage. Also experienced service observers will be more efficient than the frequently changing NPARSEC observer, but this is balanced by greater familiarity of the NPARSEC observer with the programme. For the UFPP we have observations that have simple and objective constraints and all the observations to date have been useful.

A benefit in the UFPP is the automated reduction pipeline which has been developed as part of the UKIDSS and has used literally thousands of images to calibrate the detector. The result is a robust and precise pipeline that it is impossible to compete with using the inhomogeneous and less structured SOFI archive.

Both types of programmes have different pros and cons, and the final efficiency and precision will probably be dominated by the differences in the telescope/instrument combinations. The SOFI focal plane is on-axis with 0.288 arcsec pixels, which has been stably mounted for 15 years on the NTT that has the most advanced active optics system on a 4 m-class telescope. The UFPP detector's focal plane is off-axis with 0.4 arcsec pixels, which has only been mounted for 6 years but is a fixed instrument on the longest running 4 m IR telescope. Since the parallaxes of brown dwarfs will remain the domain of ground-based programmes for the foreseeable future, this is an interesting comparison.

6.2 Large surveys and future space missions

Pan-STARRS (Kaiser et al. 2002) and the future LSST surveys (LSST Science Collaboration et al. 2009) will image the sky many times a year, automatically providing the observations for parallax determination. However, surveys are managed to maximize coverage and depth; if this is done at the expense of astrometric precision or the scheduling flexibility that parallax observations require, the final precision will suffer. The 1–2 mas precision goal we have set for NPARSEC will be challenging for these large surveys, though even lower precisions with a significantly larger sample are exciting.

The impact of future astrometric space missions is promising but uncertain. The *Japan Astrometry Satellite Mission for Infrared Exploration* (*JASMINE*; Gouda et al. 2002) will measure parallaxes for thousands of T dwarfs, but the future of that mission is not clear and the precursor, *Nano-JASMINE* (Kobayashi et al. 2005), will not observe any T dwarfs. The *Gaia* mission will determine parallaxes with errors better than 0.5 mas for all objects to *Gaia* magnitude 20 (de Bruijne 2012), but the only T dwarfs this bright are Epsilon Indi Ba and WISE J104915.57−531906.1AB (Luhman 2013). *Gaia* will discover many T dwarfs indirectly as companions of brighter objects providing an unprecedented wealth of benchmark systems. *Gaia* will provide a more precise correction from the relative to absolute parallax for ground-based parallax programmes; however, as shown in Table 3, this correction is small, so the overall precision is dominated by the internal random error. *Gaia* will also provide an accurate reference frame which, in theory, could be used to model focal plane distortions. However, providing the focal plane does not change over the observational programme; the differential nature of ground-based programmes uses the full precision of the observations while any modelling will introduce errors even with a perfect reference catalogue and the availability of improved *Gaia* accuracy may not translate into improved parallax estimates.

7 CONCLUSIONS AND FUTURE WORK

We have described the NPARSEC programme targets, instrumentation and procedures, and produced first parallaxes and proper motions for ten objects including five new objects. The observations are currently scheduled until late 2013 at which point we will publish a complete set of results. We are already finding surprises for individual targets, and we are gathering the supporting photometric and spectroscopic information to produce a complete homogenous observational data set to characterize the overall population.

ACKNOWLEDGEMENTS

The authors would like to acknowledge the Marie Curie 7th European Community Framework Programme grant n.236735, Parallaxes of Southern Extremely Cool objects (PARSEC) International Incoming Fellowship and grant n.247593, Interpretation and Parameterisation of Extremely Red COOL dwarfs (IPERCOOL) International Research Staff Exchange Scheme.

The main observational data were collected at the European Organisation for Astronomical Research in the Southern Hemisphere, Chile programme 186.C-0756. Observational data from three other programmes have been used to support this research: A22TAC_96 on the Italian Telescopio Nazionale Galileo, U09B14 on the United Kingdom Infrared Telescope and SO2012B-018 on the Southern Astrophysical Research Telescope.

The authors thank the anonymous referees for their useful comments.

REFERENCES

Andrei A. H. et al., 2011, AJ, 141, 54
Artigau É., Doyon R., Lafrenière D., Nadeau D., Robert J., Albert L., 2006, ApJ, 651, L57
Artigau É., Radigan J., Folkes S., Jayawardhana R., Kurtev R., Lafrenière D., Doyon R., Borissova J., 2010, ApJ, 718, L38
Bertin E., Arnouts S., 1996, A&A, 117, 393
Burgasser A. J., 2007, ApJ, 659, 655
Burgasser A. J. et al., 2000, AJ, 120, 1100
Burgasser A. J. et al., 2002, ApJ, 564, 421
Burgasser A. J., McElwain M. W., Kirkpatrick J. D., 2003, AJ, 126, 2487
Burgasser A. J., McElwain M. W., Kirkpatrick J. D., Cruz K. L., Tinney C. G., Reid I. N., 2004, AJ, 127, 2856
Burgasser A. J., Kirkpatrick J. D., Cruz K. L., Reid I. N., Leggett S. K., Liebert J., Burrows A., Brown M. E., 2006a, ApJS, 166, 585
Burgasser A. J., Geballe T. R., Leggett S. K., Kirkpatrick J. D., Golimowski D. A., 2006b, ApJ, 637, 1067
Burgasser A. J., Cruz K. L., Cushing M., Gelino C. R., Looper D. L., Faherty J. K., Kirkpatrick J. D., Reid I. N., 2010, ApJ, 710, 1142
Burningham B. et al., 2010, MNRAS, 404, 1952
Burningham B. et al., 2013, MNRAS, submitted
Chiu K., Fan X., Leggett S. K., Golimowski D. A., Zheng W., Geballe T. R., Schneider D. P., Brinkmann J., 2006, AJ, 131, 2722
Chiu K. et al., 2008, MNRAS, 385, L53
Cruz K. L., Burgasser A. J., Reid I. N., Liebert J., 2004, ApJ, 604, L61
Dahn C. C. et al., 2002, AJ, 124, 1170
de Bruijne J. H. J., 2012, Ap&SS, 341, 31
Delorme P. et al., 2008a, A&A, 482, 961

Delorme P. et al., 2008b, A&A, 484, 469
Devillard N., 1997, The Messenger, 87, 19
Dupuy T. J., Liu M. C., 2012, ApJS, 201, 19
Dupuy T., Kraus A., Liu M., 2011, Spitzer Proposal, 80233
Ellis S. C., Tinney C. G., Burgasser A. J., Kirkpatrick J. D., McElwain M. W., 2005, AJ, 130, 2347
Faherty J. K., Burgasser A. J., Cruz K. L., Shara M. M., Walter F. M., Gelino C. R., 2009, AJ, 137, 1
Faherty J. K. et al., 2012, ApJ, 752, 56
Geballe T. R. et al., 2002, ApJ, 564, 466
Goldman B., Marsat S., Henning T., Clemens C., Greiner J., 2010, MNRAS, 405, 1140
Gouda N. et al., 2002, in Ikeuchi S., Hearnshaw J., Hanawa T., eds, 8th Asian-Pacific Regional Meeting, Volume II, PASJ, Tokyo, p. 5
Hawley S. L. et al., 2002, AJ, 123, 3409
Jao W.-C., Henry T. J., Subasavage J. P., Winters J. G., Riedel A. R., Ianna P. A., 2011, AJ, 141, 117
Kaiser N. et al., 2002, in Tyson J. A., Wolff S., eds, Proc. SPIE Conf. Ser. Vol. 4836, Survey and Other Telescope Technologies and Discoveries. SPIE, Bellingham, p. 154
Khandrika H., Burgasser A. J., Melis C., Luk C., Bowsher E., Swift B., 2013, AJ, 145, 71
Kirkpatrick J. D. et al., 2000, AJ, 120, 447
Kirkpatrick J. D. et al., 2010, ApJS, 190, 100
Kirkpatrick J. D. et al., 2011, ApJS, 197, 19
Kirkpatrick J. D. et al., 2012, Spitzer Proposal, 90007
Knapp G. R. et al., 2004, AJ, 127, 3553
Kobayashi Y. et al., 2005, in Kurtz D. W., ed., IAU Colloq. 196: Transits of Venus: New Views of the Solar System and Galaxy. Cambridge Univ. Press, Cambridge, p. 491
Lawrence A. et al., 2007, MNRAS, 379, 1599
Lodieu N. et al., 2007, MNRAS, 379, 1423
Looper D. L., Kirkpatrick J. D., Burgasser A. J., 2007, AJ, 134, 1162
LSST Science Collaboration et al., 2009, arXiv:e-prints
Lucas P. W., Roche P. F., Allard F., Hauschildt P. H., 2001, MNRAS, 326, 695
Luhman K. L., 2013, ApJ, 767, L1
Marocco F. et al., 2010, A&A, 524, A38
Martin E. L., Brandner W., Basri G., 1999, Sci, 283, 1718
Mendez R. A., van Altena W. F., 1996, AJ, 112, 655
Moorwood A., Cuby J.-G., Lidman C., 1998, The Messenger, 91, 9
Nakajima T., Oppenheimer B. R., Kulkarni S. R., Golimowski D. A., Matthews K., Durrance S. T., 1995, Nat, 378, 463
Neuhäuser R. et al., 2002, Astron. Nachr., 323, 447
Perryman M. A. C. et al., 2001, A&A, 369, 339
Pinfield D. J. et al., 2008, MNRAS, 390, 304
Radigan J., Jayawardhana R., Lafrenière D., Artigau É., Marley M., Saumon D., 2012, ApJ, 750, 105
Reid I. N., Cruz K. L., Kirkpatrick J. D., Allen P. R., Mungall F., Liebert J., Lowrance P., Sweet A., 2008, AJ, 136, 1290
Scholz R.-D., 2010, A&A, 515, A92
Scholz R.-D., Bihain G., Schnurr O., Storm J., 2011, A&A, 532, L5
Shkolnik E. L., Anglada-Escudé G., Liu M. C., Bowler B. P., Weinberger A. J., Boss A. P., Reid I. N., Tamura M., 2012, ApJ, 758, 56
Skrutskie M. F. et al., 2006, AJ, 131, 1163
Smart R. L., 2009, Mem. Soc. Astron. Ital., 80, 674
Smart R. L., Lattanzi M. G., Drimmel R., 1997, in Kontizas E., Kontizas M., Morgan D. H., Vettolani G. P., eds, Astrophysics and Space Science Library, Vol. 212, Wide-Field Spectroscopy. Kluwer Academic Publishers, Dordrecht, p. 195
Smart R. L. et al., 2003, A&A, 404, 317
Smart R. L. et al., 2010, A&A, 511, A30
Stephens D. C., Leggett S. K., 2004, PASP, 116, 9
Stumpf M. B., Brandner W., Bouy H., Henning T., Hippler S., 2010, A&A, 516, A37
Tinney C. G., Burgasser A. J., Kirkpatrick J. D., 2003, AJ, 126, 975 (TIN03)
Tinney C. G., Burgasser A. J., Kirkpatrick J. D., McElwain M. W., 2005, AJ, 130, 2326
Tinney C. G., Faherty J. K., Kirkpatrick J. D., Wright E. L., Gelino C. R., Cushing M. C., Griffith R. L., Salter G., 2012, ApJ, 759, 60
Vrba F. J. et al., 2004, AJ, 127, 2948
Wright E. L. et al., 2010, AJ, 140, 1868
York D. G. et al., 2000, AJ, 120, 1579

This paper has been typeset from a TEX/LATEX file prepared by the author.